Nanoscale Res Lett (2010) 5:1474–1479
DOI 10.1007/s11671-010-9664-4

NANO EXPRESS

Synthesis and Magnetic Properties of Maghemite (γ-Fe_2O_3) Short-Nanotubes

W. Wu · X. H. Xiao · S. F. Zhang · T. C. Peng · J. Zhou · F. Ren · C. Z. Jiang

Received: 26 March 2010 / Accepted: 3 June 2010 / Published online: 17 June 2010

Abstract We report a rational synthesis of maghemite (γ-Fe_2O_3) short-nanotubes (SNTs) by a convenient hydrothermal method and subsequent annealing process. The structure, shape, and magnetic properties of the SNTs were investigated. Room-temperature and low-temperature magnetic measurements show that the as-fabricated γ-Fe_2O_3 SNTs are ferromagnetic, and its coercivity is nonzero when the temperature above blocking temperature (T_B). The hysteresis loop was operated to show that the magnetic properties of γ-Fe_2O_3 SNTs are strongly influenced by the morphology of the crystal. The unique magnetic behaviors were interpreted by the competition of the demagnetization energy of quasi-one-dimensional nanostructures and the magnetocrystalline anisotropy energy of particles in SNTs.

Keywords Short-nanotubes · γ-Fe_2O_3 · Magnetic properties

Introduction

In recent years, the assembled nanostructures of magnetic iron oxide materials have attracted widespread interest because of their diverse applications, such as magnetic fluids, data storage, catalyst, and bionanotechnology [1–3]. One-dimensional (1D) nanostructures are very appealing, owing to many unique physical and chemical properties based on their high intrinsic anisotropy and surface activity [4, 5]. Especially, understanding the correlation between the magnetic properties and the morphology of nanostructures is a prerequisite for widespread applications of nanomagnetism in data storage and bioseparation areas [6]. However, it is crucial to choose the materials for the construction of nanostructure materials and devices with adjustable physical and chemical properties. Among the various magnetic materials, the cubic spinel structured maghemite (γ-Fe_2O_3) represents an important class of magnetic transition metal oxide materials in which oxygen atoms form a fcc close-packed structure [7]. Moreover, γ-Fe_2O_3 is an ideal candidate for fabrication of luminescent and magnetic dual functional nano-composites due to its excellent transparent properties [8–10].

The search for new geometries is an important aspect for magnetic iron oxide nanomaterials, and past research mainly has lead to structures such as nanoparticles, hollow nanoparticles [1, 11–13]. Generally, the lowest energy state of a magnetic particle depends on its size, shape, strength and character of its anisotropy, especially the shape of nanomaterials can influence its magnetic properties in different ways. Magnetic quantities such as anisotropy and coercivity are important for many present and future applications in permanent magnetism, magnetic recording, and spin electronics [14]. More recently, the magnetic properties of nanoparticles, nanocages, nanowires, and nanochains have been reported [13, 15–18]. However, reports on the template-free synthesis and magnetic properties of γ-Fe_2O_3 SNTs are very scarce so far [8, 19, 20]. In the present work, we demonstrated an efficient and facile

W. Wu · C. Z. Jiang (✉)
Key Laboratory of Artificial Micro- and Nano-structures of Ministry of Education,
Wuhan University, Wuhan 430072, People's Republic of China
e-mail: czjiang@whu.edu.cn

W. Wu · X. H. Xiao · S. F. Zhang · T. C. Peng · J. Zhou · F. Ren · C. Z. Jiang
Center for Electronic Microscopy and School of Physics and Technology, Wuhan University, Wuhan 430072, People's Republic of China

approach for large-scale synthesis of γ-Fe_2O_3 SNTs by hydrothermal and subsequent annealing process. The scanning electron microscopy (SEM) and transmission electron microscopy (TEM) results showed that the obtained products were short-tubular structures. The room-temperature and low-temperature magnetic properties of these SNTs were investigated. The study of pure γ-Fe_2O_3 SNTs and their magnetic properties is a key issue, not only for practical applications but also for fundamental understanding.

Experimental Section

At first, the starting materials were prepared by a hydrothermal treatment of iron (III) chloride with sulfate and phosphate additives. In a typical experimental procedure, 0.27 g $FeCl_3 \cdot 6H_2O$, 7 mg $NaH_2PO_4 \cdot 2H_2O$, and 19.5 mg Na_2SO_4 aqueous solutions were mixed together and then double-distilled water was added to the mixture to keep the final volume at 25 mL. After ultrasonic dispersion, the mixture was transferred into a Teflon-lined stainless steel autoclave with a capacity of 30 mL for hydrothermal treatment at 220°C for 12 h. After the autoclave was allowed to cool to room temperature, the precipitate was separated by centrifugation, washed with double-distilled water, and dried under vacuum at 120°C. Then, as-obtained dried α-Fe_2O_3 powders were annealed in a tubular furnace at 300°C under a continuous hydrogen flow for 5 h. The furnace was allowed to cool to room temperature while still under a continuous hydrogen gas flow. Finally, the above sample was annealed at 400°C for 2 h in oxygen atmosphere with the heating rate of 5°C/min.

The morphologies and microstructures of as-synthesized samples were characterized by scanning electron microscopy (FEI Nova 400 NanoSEM), transmission electron microscopy (JEOL JEM-2010(HT)), and high-resolution transmission electron microscopy (JEOL JEM-2010 FET (UHR)). The operating voltages of the SEM and TEM were 25 and 200 kV, respectively. The crystal structure of the samples was determined by X-ray diffraction (XRD) (Cu Kα radiation, $\lambda = 0.1542$ nm). The Brunauer-Emmett-Teller (BET) surface area of the annealing samples was analyzed by nitrogen adsorption in a Micromeritics ASAP 2020 nitrogen adsorption apparatus. The composition of as-synthesized samples was measured by attenuated total reflectance Fourier transform infrared (ATR-FTIR) spectroscopy (Nicolet iS10). Magnetic measurements were performed on a Quantum Design physical property measurement system (PPMS). The powder sample was filled in a diamagnetic plastic tube, and then the packed sample was put in a diamagnetic plastic straw and impacted into a minimal volume for magnetic measurements. Background magnetic measurements were checked for the packing material.

Results and Discussion

SEM was used to confirm the morphology of as-obtained γ-Fe_2O_3 SNTs, and the SEM images (Fig. 1a) clearly show the capsule-like tubular nature of the γ-Fe_2O_3 SNTs. The rough surface of the SNTs implies that the surface is composed of closely packed and well-aligned small nanoparticles. Detailed structural information and the growth direction of the γ-Fe_2O_3 SNTs were obtained from TEM and HRTEM micrographs. Figure 1b depicts that those particles are all of hollow short-tubular morphology. It is noteworthy that some of SNTs have one end open with the other end closed. The selected area electron diffraction (SAED) patterns of the sample indicate the crystallin characteristics of maghemite aggregates (see insert in Fig. 1b). The TEM micrograpy at high magnification (Fig. 1c) clearly shows that the SNTs are composed of closely packed small nanoparticles. The corresponding HRTEM image (Fig. 1d, take from the open end of SNTs) of the selected area marked a# in Fig. 1c shows crystalline character with lattice spacing of 0.252 nm and 0.295 nm, which can be indexed to the (311) and (220) planes of cubic γ-Fe_2O_3. And the HRTEM image take from the tube wall of the selected area marked b# in Fig. 1c shows crystalline character with lattice spacing of 0.252 nm, which can be indexed to the (311) plane of cubic γ-Fe_2O_3.

The composition and phase purity of the as-prepared products were examined by X-ray diffraction (XRD). Figure 2a shows the XRD patterns of the starting materials and as-prepared γ-Fe_2O_3 SNTs. From the XRD patterns of starting materials, it can be seen that the XRD patterns conformity with that of rhombohedral α-Fe_2O_3 (JCPDS card 33-0664, show in the bottom). After annealing treatment, the (220), (311), (400), (422), (511), and (440) diffraction peaks observed at curves can be indexed to the cubic spinel structure, and all peaks are in good agreement with pure γ-Fe_2O_3 phase (JCPDS card 39–1346 is also shown in the bottom). γ-Fe_2O_3 can be prepared by the reduction and oxidation of α-Fe_2O_3 under air at $T = 523$ K [21]. This result reveals that the starting materials (α-Fe_2O_3 SNTs) have been completely change to γ-Fe_2O_3 SNTs. The attenuated total reflection Fourier transform infrared spectroscopy (ATR-FTIR) spectra of starting materials and γ-Fe_2O_3 SNTs are shown in Fig. 2b. The adsorption bands at ca. 560 cm^{-1} related to the lattice vibrations of the FeO_6 octahedral [22]. The broad bands of as-prepared samples at 700 cm^{-1} are assigned to the bending modes of Fe–O–H corresponding to Fe_2O_3 [23]. The four resolved weak adsorption peaks within 900–1050 cm^{-1} result from

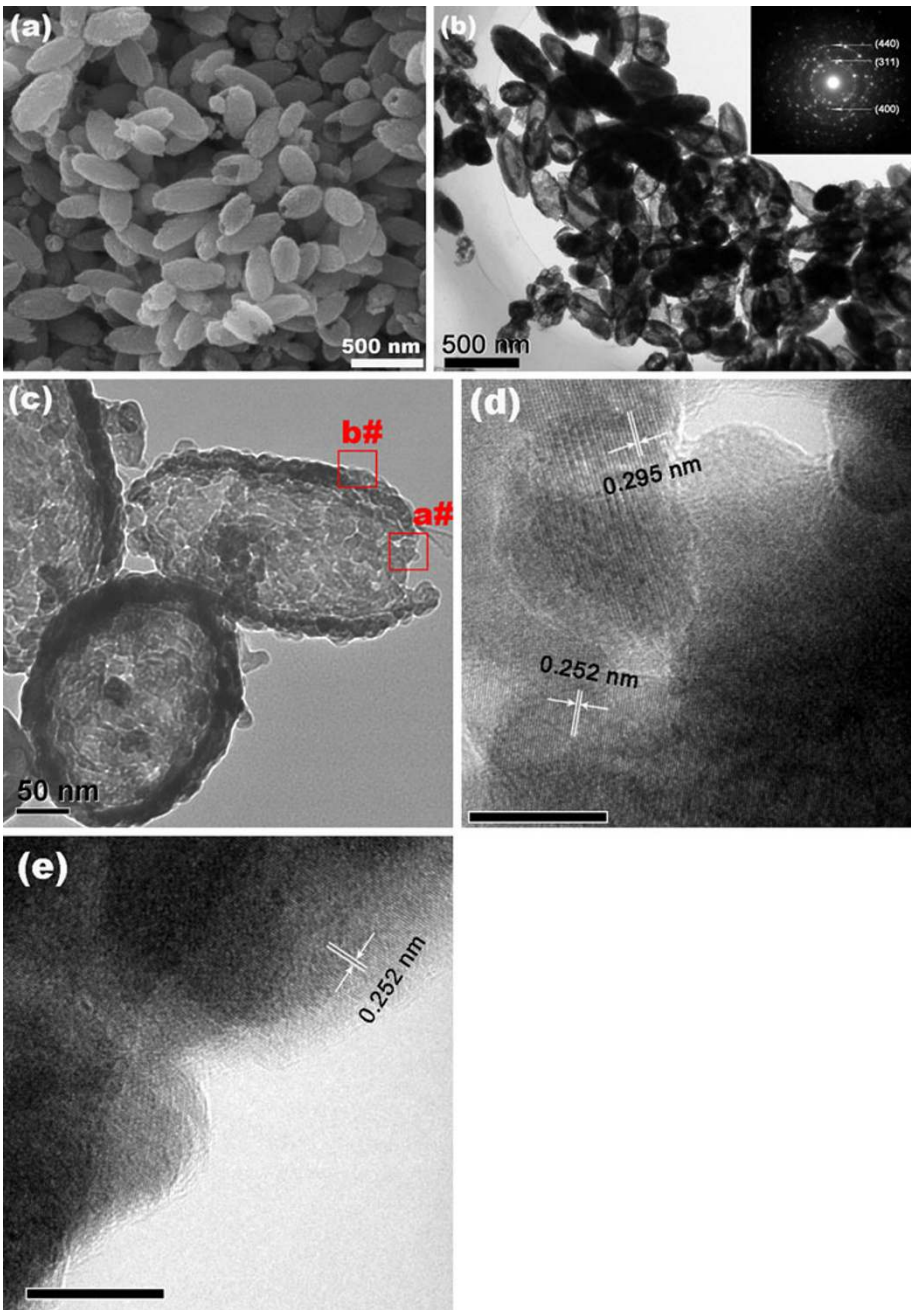

Fig. 1 SEM (**a**), TEM (**b**, **c**), and HRTEM (**d**, **e**, the *scale bar* is 10 nm) images of as-prepared γ-Fe_2O_3 SNTs

incorporated sulfate ions in the preparing process, corresponding to the one band of the $\nu 1$ mode and two bands of the $\nu 3$ mode ($C_{3\nu}$ symmetry), respectively [24]. The ATR-FTIR spectra of starting materials and γ-Fe_2O_3 SNTs show similar trends, indicating that the composition will not change by the annealing treatment.

Nitrogen adsorption and desorption measurement for determine the specific surface area and pore size for starting materials and as-prepared γ-Fe_2O_3 SNTs, the corresponding results are presented in Fig. 3. All the samples were degassed before the nitrogen adsorption measurement. The Brunauer-Emmett-Teller (BET) surface area was determined by a multipoint BET method using the adsorption data in the relative pressure (P/P_0) range of 0.05–0.3. A desorption isotherm was used to determine the pore size distribution by the Barret–Joyner–Halender (BJH) method. The nitrogen adsorption volume at the relative pressure (P/P_0) of 0.9935 and 0.9957 was used to determine the pore volume and average pore size for annealing samples. The starting materials and γ-Fe_2O_3 SNTs both exhibit a type H3 hysteresis loop according Brunauer–Deming–Deming–Teller (BDDT) classification, indicating the presence of mesopores (2–50 nm) and the pore can be assumed as a cylindrical pore mode [25, 26].

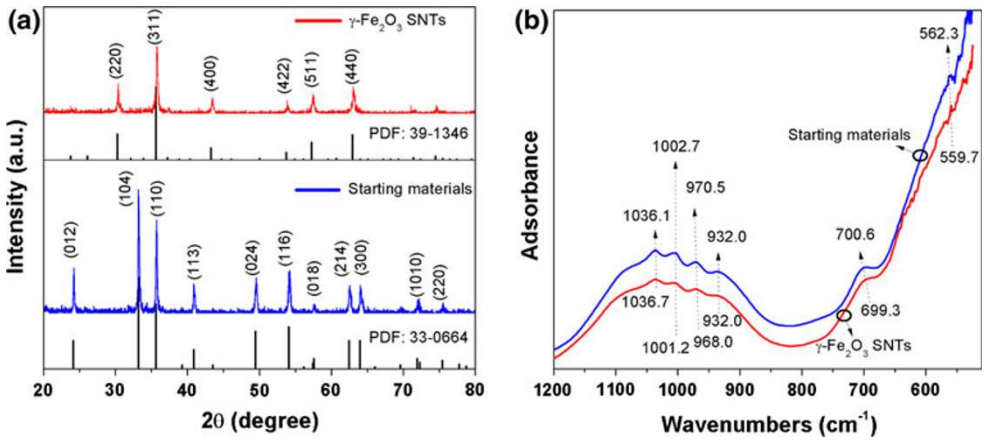

Fig. 2 XRD patterns (**a**) and ATR-FTIR spectra (**b**) of as-prepared starting materials and γ-Fe_2O_3 SNTs

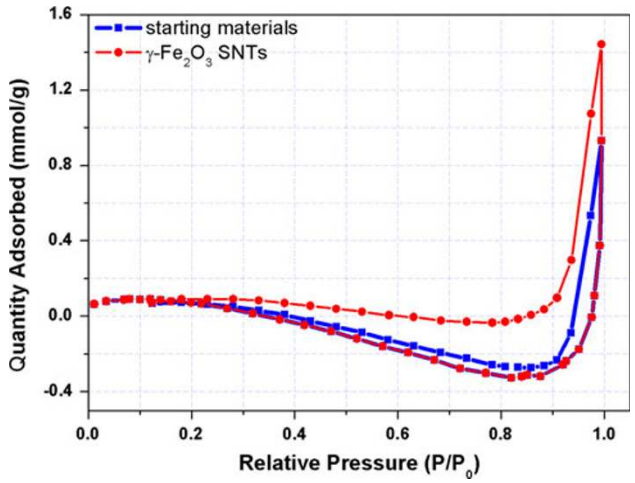

Fig. 3 Nitrogen adsorption and desorption curves of starting materials and as-prepared γ-Fe_2O_3 SNTs at 77 K

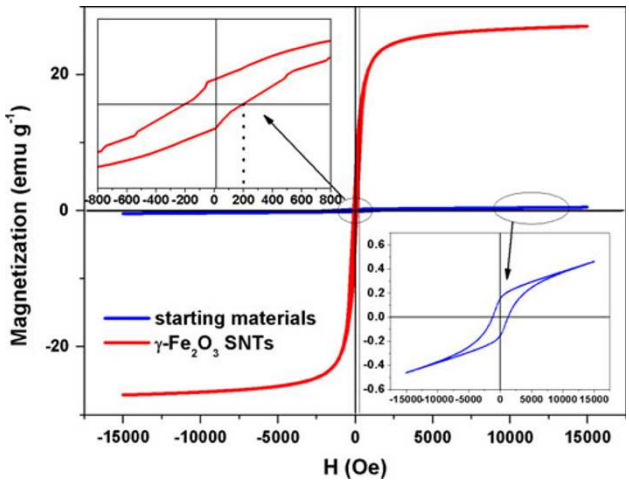

Fig. 4 Magnetic hysteresis loops at $T = 300$ K and the enlarged partial hysteresis curves for starting materials and as-prepared γ-Fe_2O_3 SNTs

According to the BET method, the specific surface area of starting materials and γ-Fe_2O_3 SNTs is 4.6288 and 9.8867 m^2/g, respectively. Moreover, the negative value of adsorbed quantity reveals that tubular nanostructure have litter or almost no micropores. The BJH adsorption cumulative pore volume of starting materials and γ-Fe_2O_3 SNTs is 0.032 and 0.050 cm^3/g, respectively (between 17 nm and 3000 nm width). The BJH desorption cumulative pore volume results are in agreement with the BJH adsorption cumulative pore volume results. The increase in the effective surface area of the SNTs was showed to be caused by the reorganization of small iron oxide nanoparticles, which may lead to the opening of some closed nanotubes in the annealing process. This is in accordance with the fact that the total pore volume of γ-Fe_2O_3 SNTs is also increased.

The room-temperature magnetic hysteresis measurements of the samples obtained at before and after the annealing process were carried out at 300 K in the applied magnetic field sweeping from −15 to 15 kOe. As shown in Fig. 4, the saturation magnetization (M_S) of starting materials and as-prepared γ-Fe_2O_3 SNTs were found to be 0.5 and 27.3 emu g^{-1} at 300 K, respectively. The increase in the saturation magnetization is most likely attributed to the phase changes from hematite (α-Fe_2O_3) to maghemite (γ-Fe_2O_3). Notably, the starting materials display a remanent magnetization (M_r) of 0.16 emu g^{-1} and coercivity (H_C) of 1030 Oe. However, the as-prepared γ-Fe_2O_3 SNTs with the M_r and H_c being determined to be 6 emu/g and 100 Oe, respectively, suggest that the γ-Fe_2O_3 SNTs exhibit weak ferromagnetic and soft magnetic behaviors [26]. The structure of α-Fe_2O_3 can be described as consisting hcp arrays of oxygen ions stacked along the [001] direction. Two-thirds of the sites are filled with Fe^{III} ions which are arranged regularly with two filled sites being followed by one vacant site in the (001) plane thereby forming sixfold rings. The structure of γ-Fe_2O_3 consists of octahedral and mixed tetrahedral/octahedral layers stacked along [111]

direction. All or most of Fe in the trivalent state, and the cation vacancies compensate for the oxidation of Fe^{II} [27]. The different valence states and cation distribution in the α-Fe_2O_3 and γ-Fe_2O_3 spinel lattice will cause the change of saturation magnetization, remnant magnetization, and coercivity [13, 21].

The magnetization curves were measured as a function of temperature with different applied fields between 10 and 300 K using field-cooling (FC) and zero-field-cooling (ZFC) procedures. In the ZFC measurements, the samples were cooled from 300 to 10 K without applying an external field. After reaching 10 K, a external field was applied, and the magnetic moments were recorded as the temperature increased. For FC measurements, the samples were cooled from 300 K under an applied external field, and then the magnetic moments were recorded as the temperature increased. As seen in Fig. 5, when the sample is cooled to the zero magnetic field temperature, the total magnetization of the SNTs will be zero since the magnetization of the individual SNTs is randomly oriented. An external magnetic field energetically favors the reorientation of the moments of the individual particles along the applied field at low temperatures. Thus, upon increasing the temperature, all the ZFC magnetic moments increase and reach a maximum, where the temperature is referred to as the blocking temperature (T_B). T_B is defined as the temperature at which the nanoparticles' moments do not relax (known as blocked) during the time scale of the measurement [16, 28]. It can be seen that blocking temperature decreases from 275 to 40 K when the applied field increases from 500 to 5000 Oe because high field can lower the energy barriers between the two easy axis orientations and

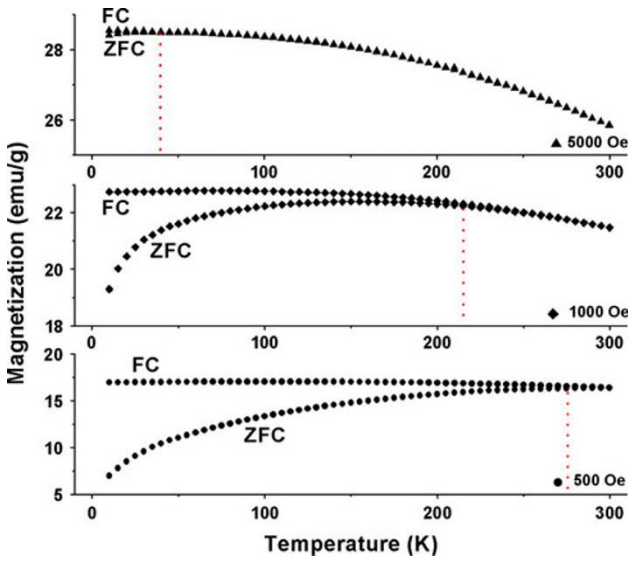

Fig. 5 Temperature dependence of ZFC and FC magnetic moments of γ-Fe_2O_3 SNTs at different applied fields

therefore lower the blocking temperature. Moreover, if the applied field reaches a critical value, the blocking temperature will disappear [29].

It is well know that the coercivity H_C is normally zero above T_B, combined the result from M–H (Fig. 4) and M–T curves (Fig. 5), one can notice that T_B of as-obtained samples at different applied fields is below 300 K. However, H_C at 300 K for γ-Fe_2O_3 SNTs is non zero, this kind of remanent magnetization and coercivity above have also been observed on the other iron oxide nanostructural materials [16, 18, 30]. This property is interesting and has not been understood well till now. For the magnetic SNTs, clear Curie–Weiss behavior is not observed above T_B and may be indicative of the existence of dipole–dipole interaction between the particles. Such behavior has been reported for several particle systems, in agreement with theoretical predictions [31–33]. Additionally, the coercivity H_C should be determined by competition of the demagnetization energy, which results from the shape anisotropy of quasi-tube nanostructure and the magnetocrystalline anisotropy energy of the particles, the coercivity can be written as follows [16, 34, 35]:

$$H_C = \frac{4L_{ex}^2 q^2 M_S}{D^2} + \frac{pcK_1^2 d^2}{M_S A} \quad (1)$$

where the first term results from the contribution of shape anisotropy energy of SNTs and the second term is due to the contribution of magnetic crystalline anisotropy energy of small particles. In the Eq. 1, here the q is the geometric factor (for a prolate spheroid, q varies between the limits of 2.0816 for a sphere and 1.8412 for an infinite cylinder, and for an oblate sphere, q gradually increases from 2.0816 for a sphere to 2.115 for an infinite plate [36]), D is the average diameter of the SNTs, d is the small particle diameter, K_1 is the first-order magnetic anisotropy constant (4.6 kJ/m^3 for γ-Fe_2O_3 [37]), A is the exchange stiffness constant ($A = 10^{-11}$ J/m), p_C is a coefficient of dimensionless quantity related to the crystal structure ($P_C \sim 0.5$), and l_{ex} is the exchange length $\left(L_{ex} = \sqrt{A/K_1} = 46.6\,\text{nm}\right)$. According to Eq. 1, the coercivity was estimated and the values was about 82 Oe. This result indicates that the coercivity of γ-Fe_2O_3 SNTs was mainly originated from the small nanocrystallines. Moreover, taking account into that T_B is defined as $T_B = K_A V/25k_B$, where K_A is the magnetic anisotropy constant, V is the magnetic core volume, and k_B is the Boltzmann constant [38]. The total magnetic core volume will decrease with the increase in applied field. Because the saturation magnetic flux density is small, such materials are easily magnetically saturated, thereby making it impossible to reduce their volumes. In other words, magnetic core volume is the most significant factor determining the inductance value, and the size and

thickness reductions are difficult to be attained unless the magnetic properties of magnetic materials are improved [39].

Conclusions

The approach used in this study provides a simple and inexpensive method for the preparation of stable and magnetic γ-Fe_2O_3 SNTs. The as-synthesized SNTs are ferromagnetic at room temperature, which may have potential applications in biotechnology, biomedicine, and fundamental science. The results reveals that the self-assembly strategy is an efficient way to create novel nanostructured systems. Further detailed studies on the formation mechanism of the magnetic SNTs are currently under investigation.

Acknowledgment The author thanks the National Basic Research Program of China (973 Program, No. 2009CB939704), the National Nature Science Foundation of China (No. 10775109, 10905043), the Specialized Research Fund for the Doctoral Program of Higher Education (No. 20070486069), Young Chenguang Project of Wuhan City (No. 200850731371, 201050231055), the Specialized Research Fund for the Young Teacher of Wuhan University(No. 1082010) and the PhD candidates self-research (including 1 + 4) program of Wuhan University in 2008 (No. 20082020201000008) for financial support.

References

1. W. Wu, Q.G. He, C.Z. Jiang, Nanoscale Res. Lett. **3**, 397 (2008)
2. S. Laurent, D. Forge, M. Port, A. Roch, C. Robic, L.V. Elst, R.N. Muller, Chem. Rev. **108**, 2064 (2008)
3. M. Faraji, Y. Yamini, M. Rezaee, J. Iran. Chem. Soc. **7**, 1 (2010)
4. S.V.N.T. Kuchibhatla, A.S. Karakoti, D. Bera, S. Seal, Prog. Mater. Sci. **52**, 699 (2007)
5. L.R. Meng, W. Chen, C. Chen, H. Zhou, Q. Peng, Y. Li, Cryst. Growth Des. **10**, 479 (2009)
6. S. Bharathi, D. Nataraj, M. Seetha, D. Mangalaraj, N. Ponpandian, Y. Masuda, K. Senthil, K. Yong, Crystengcomm **12**, 373 (2010)
7. R.C. O'Handley, *Modern Magnetic MaterialsOPrinciples and Applications* (New York, Wiley, 2000)
8. H.M. Fan, J.B. Yi, Y. Yang, K.W. Kho, H.R. Tan, Z.X. Shen, J. Ding, X.W. Sun, M.C. Olivo, Y.P. Feng, Acs Nano **3**, 2798 (2009)
9. R.F. Ziolo, E.P. Giannelis, B.A. Weinstein, M.P. O'horo, B.N. Ganguly, V. Mehrotra, M.W. Russell, D.R. Huffman, Science **257**, 219 (1992)
10. D. Wang, F. Qian, C. Yang, Z.H. Zhong, C.M. Lieber, Nano Lett. **4**, 871 (2004)
11. W. Wu, Q.G. He, R. Hu, J.K. Huang, H. Chen, Rare Met. Mater. Eng. **36**, 238 (2007)
12. S. Peng, S.H. Sun, Angew. Chem. Int. Ed. **46**, 4155 (2007)
13. W. Wu, X.H. Xiao, S.F. Zhang, H. Li, X.D. Zhou, C.Z. Jiang, Nanoscale Res. Lett. **4**, 926 (2009)
14. Y.C. Sui, R. Skomski, K.D. Sorge, D.J. Sellmyer, J. Appl. Phys. **95**, 7151 (2004)
15. K. Woo, J. Hong, S. Choi, H.-W. Lee, J.-P. Ahn, C.S. Kim, S.W. Lee, Chem. Mater. **16**, 2814 (2004)
16. L.Y. Zhang, Y.F. Zhang, J. Magn. Magn. Mater. **321**, L15 (2009)
17. K. Nakata, Y. Hu, O. Uzun, O. Bakr, F. Stellacci, Adv. Mater. **20**, 4294 (2008)
18. S.M. Zhou, X.T. Zhang, H.C. Gong, B. Zhang, Z.S. Wu, Z.L. Du, S.X. Wu, J. Phys.-Condens. Mat. **20**, 075217 (2008)
19. C.J. Jia, L.D. Sun, F. Luo, X.D. Han, L.J. Heyderman, Z.G. Yan, C.H. Yan, K. Zheng, Z. Zhang, M. Takano, N. Hayashi, M. Eltschka, M. Klaui, U. Rudiger, T. Kasama, L. Cervera-Gontard, R.E. Dunin-Borkowski, G. Tzvetkov, J. Raabe, J. Am. Chem. Soc. **130**, 16968 (2008)
20. C.J. Jia, L.D. Sun, Z.G. Yan, L.P. You, F. Luo, X.D. Han, Y.C. Pang, Z. Zhang, C.H. Yan, Angew. Chem. Int. Ed. **44**, 4328 (2005)
21. I. Mitov, Z. Cherkezova-Zheleva, V. Mitrov, Phys. Status Solidi. A **161**, 475 (1997)
22. X.O. Wang, L.S. Gao, H.G. Zheng, M.R. Ji, T. Shen, Z. Zhang, J. Cryst. Growth **269**, 489 (2004)
23. S. Mitra, S. Das, K. Mandal, S. Chaudhuri, Nanotechnology **18**, 275608 (2007)
24. T. Sugimoto, Y. Wang, J. Colloid Interface Sci. **207**, 137 (1998)
25. K.S.W. Sing, Ra.W. Haul, L. Moscou, R.A. Pierotti, J. Rouquerol, T. Siemieniewska, Pure Appl. Chem. **57**, 603 (1985)
26. W. Wu, X.H. Xiao, S.F. Zhang, L.X. Fan, T.C. Peng, F. Ren, C.Z. Jiang, Nanoscale Res. Lett. **5**, 116 (2010)
27. R.M. Cornell, U. Schwertmann, *The iron oxides: Structure, properties, reactions, occurences and used* (Wiely-VCH, USA, 2003)
28. Y.L. Hou, S. Gao, T. Ohta, H. Kondoh. Eur. J. Inorg. Chem., 1169, (2004)
29. Q. Chen, Z.J. Zhang, Appl. Phys. Lett. **73**, 3156 (1998)
30. Y.Y. Xu, X.F. Rui, Y.Y. Fu, H. Zhang, Chem. Phys. Lett. **410**, 36 (2005)
31. E. Del Barco, J. Asenjo, X.X. Zhang, R. Pieczynski, A. Julia, J. Tejada, R.F. Ziolo, D. Fiorani, A.M. Testa, Chem. Mater **13**, 1487 (2001)
32. R.W. Chantrell, N.S. Walmsley, J. Gore, M. Maylin, J. Appl. Phys. **85**, 4340 (1999)
33. L. Wang, J. Ding, H.Z. Kong, Y. Li, Y.P. Feng, Phys. Rev. B **64**, 214410 (2001)
34. S. Thomas, S.H. Al-Harthi, D. Sakthikumar, I.A. Al-Omari, R.V. Ramanujan, Y. Yoshida, M.R. Anantharaman, J. Phys. D Appl. Phys. **41**, 155009 (2008)
35. G. Herzer, IEEE Trans. Magn. **26**, 1397 (1990)
36. O. Kitakami, Y. Shimada, Jpn. J. Appl. Phys. **40**(Part 1), 4019 (2001)
37. D.L. Hou, X.F. Nie, H.L. Luo, Appl. Phys. A **66**, 109 (1998)
38. X.F. Zheng, S.L. Yuan, Z.M. Tian, S.Y. Yin, J.H. He, K.L. Liu, L. Liu, Chem. Mater. **21**, 4839 (2009)
39. I. Nowik, W. Semmler, S. Molodtsov, Hyperfine Interact. **112**, 77 (1998)